Hindawi
Geofluids
Volume 2022, Article ID 6778076, 14 pages
https://doi.org/10.1155/2022/6778076

Research Article

Properties and Engineering Applications of a New Goaf Grouting Filling Material

Xiao Feng,[1] **Chong Xia**,[1] **Sifeng Zhang**,[1] **Chuangui Li**,[2] **Hongkui Zhao**,[2] **Jianfeng Wu**,[2] **Mengjun Chen**,[3] **and Jia Yan**[4]

[1]*School of Transportation Engineering, Shandong Jianzhu University, Jinan, 250101 Shandong, China*
[2]*Shandong Luqiao Group Co., Ltd., Jinan, 250021 Shandong, China*
[3]*School of Qilu Transportation, Shandong University, Jinan, 250061 Shandong, China*
[4]*Research Center of Geotechnical and Structural Engineering, Shandong University, Jinan, 250061 Shandong, China*

Correspondence should be addressed to Xiao Feng; feng_xiao902@163.com

Received 13 July 2021; Revised 22 November 2021; Accepted 9 December 2021; Published 11 January 2022

Academic Editor: Dan Ma

In the treatment of goafs in traffic engineering, technical problems such as those related to large-volume grouting and the precise control of material properties are often encountered. To address these issues, we developed a new composite material comprising cement-fly ash-modified sodium silicate (C-FA-MS). The setting time, fluidity, unconfined compressive strength, and microstructure were varied for different proportions of cement-sodium silicate (C-S) slurry, cement-fly ash-sodium silicate (C-FA-S) slurry, and C-FA-MS slurry, and their performances were compared and analysed. The experimental results showed that the initial setting time of the slurry was the shortest when both the original sodium silicate volume ratio (V_S) and modified sodium silicate volume ratio (V_{MS}) were 0.2. The final setting time of the C-S and C-FA-S slurries tended to decrease but then increased with decrease in V_S, while that of the C-FA-MS slurry increased with lower V_{MS}. The fluidity of the C-FA-S and C-FA-MS slurries decreased with decrease in V_S or V_{MS} at different fly ash admixture ratios. The consolidation compressive strength of C-S increased with decreasing V_S, while that of C-FA-S showed a considerable increase only when V_S decreased from 0.4 to 0.2. Meanwhile, the compressive strength of the C-FA-MS concretions first increased and then decreased with decrease in V_{MS}. Microstructural analysis revealed that there were more cracks in the C-S agglomerate, the fly ash in the C-FA-S agglomerate reduced the relative density of the skeletal structure, and the stronger cross-linking in the C-FA-MS agglomerate improved the strength of the agglomerate. Under the condition of unit grouting volume, the cost of the C-FA-MS slurry was approximately 44.7% and 31.3% lower than that of the C-S and C-FA-S slurries, respectively. The new C-FA-MS material was applied for the treatment of the goaf in the Wu Sizhuang coal mine. Core drilling detection and audiofrequency magnetotelluric survey revealed that the goaf was sufficiently filled.

1. Introduction

Coal is the most widely distributed fossil energy resource worldwide. Currently, it is still one of the main energy sources for industrial production and social life in China, and it is expected that its use will continue for a long time in the future. A large number of old and new mined-out areas are formed, owing to the increasing demand for energy, in the process of coal mining, which may lead to surface collapse. With stricter regulation of "Belt and Road Initiative (BRI)" and the "Building China's Strength in Transportation" national strategies, China's transportation infrastructure has developed rapidly. However, the construction of railroads, highways, subways, and other transportation facilities frequently encounters these mined-out regions, which may lead to various types of mining collapse areas, leading to technical problems such as road structure stability, settlement deformation control, and effective filling

of goaf, along with severe regulations of ecological environmental protection and threat to the safety of people's lives and properties [1, 2].

Treatment methods such as caving, grouting reinforcement, and filling are typically used to deal with various types of goafs [3]. Among them, the grouting method is commonly used for the treatment of mined-out areas of traffic engineering by filling holes, strengthening rock and soil masses, and using advanced technologies. Ma et al. [4, 5] studied the non-Darcy hydraulic properties and deformation behaviours of granular gangue in laboratory, in theory, and in situ. They effectively evaluated the reuse of gangue wastes by gangue backfilling mining (GBM) and its advantages in overburden aquifer protection. Moreover, a series of point bending tests were carried out on granite disc samples with the same diameter but different heights. Acoustic emission experiments were then performed to study the effect of the height/diameter ratio (H/D) on the failure properties and damage characteristics of the samples under coupled bending and splitting deformation. Liu et al. [6] established a mechanical model of grouting reinforcement for fractured rock mass and analysed the influence of factors such as the degree of rock mass fragmentation and bonding performance of grouting materials on the solidification strength. They also proposed a formula for calculating the strength of reinforced solids to better predict the reinforcement strength of a fractured rock mass. Qing-song et al. [7] studied the grouting diffusion law of cement-sodium silicate slurry in flowing water, providing valuable insights for guiding the design and construction of grouting to deal with water inrush disasters. Xuan et al. [8] designed a set of long-wall overburden grouting visualisation experimental simulation systems to study the flow, pressure distribution, consolidation, and filling thickness of fly ash slurry in rock strata, providing a theoretical basis for the design and optimisation of overburden grouting in underground long-wall mining. Girskas et al. [9] studied the effective utilisation of fly ash and demonstrated that this material can inhibit the cement hydration process and can be used to produce cement-based composite materials with better frost resistance and durability. Gorak et al. [10] used composite lightweight aggregates (such as fly ash) to partially replace natural aggregates in cement composite materials. They concluded that reducing the water content in the mixture while maintaining good workability can increase the compressive and flexural strength by up to 25% than that of standard mortar. Hu et al. [11] proposed a new grouting material with a high water content expansion material to consolidate and block boreholes and studied the injectability, compression resistance, and bondability of grouting materials. Sukmak et al. [12] added natural rubber to cement and examined its influence on the setting time, compressive strength, bending strength, and toughness of the consolidation. Ma et al. [13] proposed a cement-gypsum-silicate grouting material and determined parameters such as strength, viscosity, and setting time for different proportions of the material using orthogonal experiments. Kumar et al. [14] investigated the hydration of Portland cement mixed with 20% fly ash in the presence of 0.1% superplasticizer by measuring the viscosity, setting time, compressive strength, and water permeability. Wang et al. [15] proposed a grouting method to prevent safety hazards using a new cement-based grouting material in a thick coal seam. Celik et al. [16] studied the rheological properties of cement grout mixed with bottom ash as a mineral additive and its influence on penetration grouting.

In the management of the goaf under traffic engineering, there are several technical difficulties, such as the precise control of material properties, and the complex situation of residual goaf. Portland cement grout has a high setting time, and its diffusion range is difficult to control. In addition, in the case of large-volume filling, Portland cement is expensive [17]. Although utilising existing solid-waste filling materials can reduce the cost of goaf filling, the compressive strength of the solid waste after coagulation is generally low, which makes it difficult for the solid waste to resist the subsidence deformation of the goaf [18]. Therefore, it is essential to investigate the physical and mechanical properties and engineering applications of a new cement-fly ash-modified sodium silicate (C-FA-MS) material as well as conduct a cost analysis of the new material. In this study, the optimum ratio, initial and final setting time, unconfined uniaxial compressive strength, and microstructure of the new material were analysed through laboratory tests. The new material was applied to the treatment project of the residual goaf, and it ensured operational safety of the overburden expressway. Moreover, it decreased the construction cost and provided a reference value for similar projects.

2. Materials and Methods

2.1. Raw Materials. P.O.42.5 Cement (C): P.O.42.5 grade ordinary Portland cement produced by Linyi Zhonglian Cement Co., Ltd. (the company is located in Chewang Town, Linyi City, Shandong Province) met the requirements of the current national standards General Portland Cement (GB 175-2007) and Masonry Cement (GB/T 3183-2017). Chemical compositions of the cement are listed in Table 1.

Fly ash (FA): commercial II grade fly ash has a fineness of 43 μm, density of approximately 2.4 g/cm^3, and moisture content of approximately 5%. The main chemical components are listed in Table 2.

Modified sodium silicate (MS): sodium silicate was modified following previously reported methods [19–21], in the following manner: deionised water was heated to 60–70°C, and then, PEG and AA were added concurrently (see Table 3 for detailed information regarding the proportions). After the mixture was cooled to 20–25°C, sodium silicate was added with continuous stirring. The matching ratio of the modified sodium silicate is shown in Table 3.

2.2. Test Mix Ratio Design. The volume mix ratio of the cement slurry-sodium silicate solution (C-S) grout is shown in Table 4, the construction mix ratios of the cement-fly ash-sodium silicate (C-FA-S) grout are shown in Table 5, and cement-fly ash-modified sodium silicate (C-FA-MS) grout is shown in Table 6. The selection of the water–solid ratio (mass ratio of water to solid powder) was based on the related research of domestic and foreign scholars [16, 18]; thus, the water–solid mass ratio was set to 1.0 : 1.0.

Table 1: Chemical composition of the cement.

Name	CaO	SiO_2	Al_2O_3	Fe_2O_3	MgO	$MgCl_2$	SO_3	NaO_2	K_2O
Content (%)	62.07	22.64	4.50	3.10	2.68	1.81	1.75	0.80	0.65

Table 2: Chemical composition of the fly ash.

Name	SiO_2	Al_2O_3	Fe_2O_3	CaO	K_2O	TiO_2	MgO	Other compositions
Content (%)	53.97	31.15	4.16	4.01	2.04	1.13	1.01	2.53

Note: Other compositions include Na_2O, SO_3, P_2O_5, and NiO. Sodium silicate (S): sodium silicate solution with a modulus of 2.4–3.0 and Baume degrees ≥ 30 °Bé. Ethylene glycol (PEG, purity ≥ 99%) and adipic acid (AA) were used for laboratory analyses.

Table 3: Modified sodium silicate (MS) matching ratio (mass proportion).

Name	Water (60–70°C)	Sodium silicate	Adipic acid	Ethylene glycol
Content (%)	65.57	32.79	0.98	0.66

Table 4: Cement slurry-sodium silicate (C-S) volume ratio.

No.	Slurry volume ratio Water-cement ratio	$V_C : V_S$
1	1.0 : 1.0	1.0 : 1.0
2		1.0 : 0.6
3		1.0 : 0.4
4		1.0 : 0.2

Note: The water-cement ratio is the mass ratio of water to cement powder; $V_C : V_S$ is the volume ratio of pure cement grout to pure sodium silicate.

2.3. Analysis of the Physical and Mechanical Properties of the Slurry

2.3.1. Setting Time Analysis. Setting time is an important property of a grouting material and considerably influences the diffusion distance of the slurry in rock and soil mass [22]. Different mass proportions of solid powder, pure sodium silicate volume dosages, and modified sodium silicate volume dosages were used to investigate the differences in the setting periods of the C-S, C-FA-S, and C-FA-MS slurries.

Determination of initial setting time: first, two empty cups A and B were selected, and 200 mL of the mixed slurry was quickly prepared in cup A. Second, the mixed slurry was poured into cup B and exchanged between cups A and B until the slurry no longer flowed, and the time elapsed was determined as the initial setting time.

Determination of the final setting time: an appropriate amount of the mixed slurry was poured into the mould of a Vicat apparatus. Immediately after the initial setting time, the mould and slurry were removed from the glass plate and cured under standard conditions (20 ± 2°C, humidity ≥ 95 %). The solidification body of the mixed slurry was measured every 10 s when the final setting time was near. When the test needle was inserted into the solidification body by 0.5 mm, we observed that the mixed slurry reached the final setting state. The curves of the initial and final setting times are shown in Figures 1 and 2, respectively.

As shown in Figure 1, the initial setting time of the slurry decreased with a decrease in V_S for pure sodium silicate or in V_{MS} for the modified sodium silicate. When both V_S and V_{MS} were 0.2, the initial setting time of the slurry was the shortest. The initial setting time increased with increase in fly ash content. For example, for $V_{(C+FA)} : V_{MS} = 1.0 : 1.0$, the initial setting time was 30 s for $m_C : m_{FA} = 60\% : 40\%$, 38 s for $m_C : m_{FA} = 50\% : 50\%$, 66 s for $m_C : m_{FA} = 40\% : 60\%$, and 120 s for $m_C : m_{FA} = 30\% : 70\%$. Moreover, when the mass ratio of the powder and the volume ratio of the slurry were constant, the initial setting time of the C-FA-MS slurry was lesser than those of the C-FA-S and C-S slurries.

Figure 2 shows that the final setting time of the C-S and C-FA-S slurries tended to shorten and then prolong with a decrease in V_S. It also increased with increase in the mass content of fly ash. When $V_{(C+FA)} : V_S = 1.0 : 0.6$, the final setting time of the slurry was the shortest. However, the final setting time of the C-FA-MS slurry increased with decrease in the volume content of modified sodium silicate (V_{MS}) and increase in the mass content of fly ash. When $m_C : m_{FA} = 60\% : 40\%$ and $V_{(C+FA)} : V_{MS} = 1.0 : 1.0$, the final setting time of the C-FA-MS slurry was the shortest, that is, 70 min.

Clearly, the effect of the rapid setting between the pure sodium silicate and the modified sodium silicate differed according to the analysis of the final setting time. We inferred that because of the reduced content of $Na_2O{\cdot}nSiO_2$ in modified sodium silicate, the amount of its reaction with CaO, Al_2O_3, and other components reduced under the same volume dosage condition, resulting in prolonged final setting time. In addition, the initial and final setting periods of the mixed slurry increased with increase in the fly ash content because the addition of fly ash reduced the content of CaO in the solid powder.

2.4. Fluidity Analysis. A concentric circle cardboard with increasing radius (equal increments) was placed on a horizontal plane, and a glass plate wiped with a damp cloth was placed above it. The mould was placed in the centre of the glass plate, and the slurry was quickly injected into it.

Table 5: Volume ratio of cement-fly ash-sodium silicate slurry (C-FA-S).

No.	Ratio of water-cement and fly ash	Ratio of slurry volume $m_C : m_{FA}$ (%)	$V_{(C+FA)} : V_S$
5	1.0 : 1.0	60 : 40	1.0 : 1.0
6			1.0 : 0.6
7			1.0 : 0.4
8			1.0 : 0.2
9		50 : 50	1.0 : 1.0
10			1.0 : 0.6
11			1.0 : 0.4
12			1.0 : 0.2
13		40 : 60	1.0 : 1.0
14			1.0 : 0.6
15			1.0 : 0.4
16			1.0 : 0.2
17		30 : 70	1.0 : 1.0
18			1.0 : 0.6
19			1.0 : 0.4
20			1.0 : 0.2

Table 6: Volume ratio of cement-fly ash-MS slurry (C-FA-MS).

No.	Ratio of water-cement and fly ash	Volume ratio of slurry $m_C : m_{FA}$ (%)	$V_{(C+FA)} : V_{MS}$
21	1.0 : 1.0	60 : 40	1.0 : 1.0
22			1.0 : 0.6
23			1.0 : 0.4
24			1.0 : 0.2
25		50 : 50	1.0 : 1.0
26			1.0 : 0.6
27			1.0 : 0.4
28			1.0 : 0.2
29		40 : 60	1.0 : 1.0
30			1.0 : 0.6
31			1.0 : 0.4
32			1.0 : 0.2
33		30 : 70	1.0 : 1.0
34			1.0 : 0.6
35			1.0 : 0.4
36			1.0 : 0.2

Note: The ratio of water-cement and fly ash is the mass ratio of water to the cement and fly ash powders; $m_C : m_{FA}$ is the mass ratio of cement to fly ash in solid powder; $V_{(C+FA)} : V_S$ is the volume ratio of cement-fly ash slurry to pure sodium silicate solution; $V_{(C+FA)} : V_{MS}$ is the volume ratio of cement-fly ash slurry to modified sodium silicate solution.

The test mould was lifted vertically, and the stopwatch was turned on at the same time. After 30 s, the maximum diameters of two mutually perpendicular directions were taken with a straight edge, and their average value was taken as the fluidity of the mixed slurry. The fluidity measurements and curves are shown in Figures 3 and 4, respectively.

Figure 4 shows that when $m_C : m_{FA} = 100\% : 0\%$, the fluidity of the cement-sodium silicate slurry increased and then decreased with decrease in V_S (the fluidity increased from 285 to 345 mm and then decreased to 325 mm). Under all blending conditions of fly ash, the fluidities of the cement-fly ash-sodium silicate and cement-fly ash-modified sodium silicate slurries decreased with a decrease in V_S or V_{MS}. When the volume ratio of the slurry was less than 1.0 : 0.4, the fluidity of the cement-fly ash-modified sodium silicate slurry was greater than that of the cement-fly ash-sodium silicate and cement-sodium silicate slurries under certain conditions. We inferred that the concentration of $Na_2O{\cdot}nSiO_2$ decreased when a large amount of water was added to the modified sodium silicate. The fluidity of the cement-fly ash-modified sodium silicate slurry increased for the same matching ratio.

2.5. Strength Analysis of Reinforcement. Referring to the ISO method for testing the strength of cement mortar (GB/T 17671-2020), the prepared mixed slurry was quickly filled into a $\Phi 50\,\text{mm} \times 100\,\text{mm}$ cylindrical test mould. If necessary, the vibrating rod was used to vibrate uniformly from the outside to the inside according to the spiral direction. Meanwhile, the scraper was inserted along the test mould wall several times to prevent the mixed slurry from leaving air holes after vibrating. The slurry should be 6–8 mm higher than the top surface of the mould before being scraped flat with a scraper.

Two samples were prepared using the ratio of each test group. Using a standard curing chamber ($20 \pm 2^{\circ}\text{C}$, humidity ≥ 95%), the samples were first cured in a test mould for 1 d. After being demoulded, the samples were cured for another 6 d (total age of 7 d). Then, the samples were removed, and the free water visible on the surface was absorbed with a soft cloth. The uniaxial compressive strength was measured at the maximum rated load of 100 kN and a loading speed of 1.66 mm/h, as shown in Figure 5.

The influences of different powder mass ratios, volume ratios of pure sodium silicate V_S, and volume ratios of modified sodium silicate V_{MS} on the unconfined compressive strength of the solidified bodies for 7 d are shown in Figure 6.

Figure 6 shows that in the cement-sodium silicate slurry system, with a decrease in V_S, the 7 d compressive strength of the solidified body exhibited an overall increasing trend. When $V_C : V_S = 1.0 : 0.2$, the maximum compressive strength reached 11.156 MPa. In the cement-fly ash-sodium silicate slurry system, the 7 d compressive strength of the solidified body showed inconspicuous changes when V_S was large. Only when V_S decreased from 0.4 to 0.2, the compressive strength increased significantly. When $m_C : m_{FA} = 60\% : 40\%$ and $V_{(C+FA)} : V_S = 1.0 : 0.2$, the maximum compressive strength could reach 10.369 MPa. In the cement-fly ash-modified sodium silicate slurry system, with a decrease in V_{MS}, the 7 d compressive strength of the solidified body first increased and then decreased. For example,

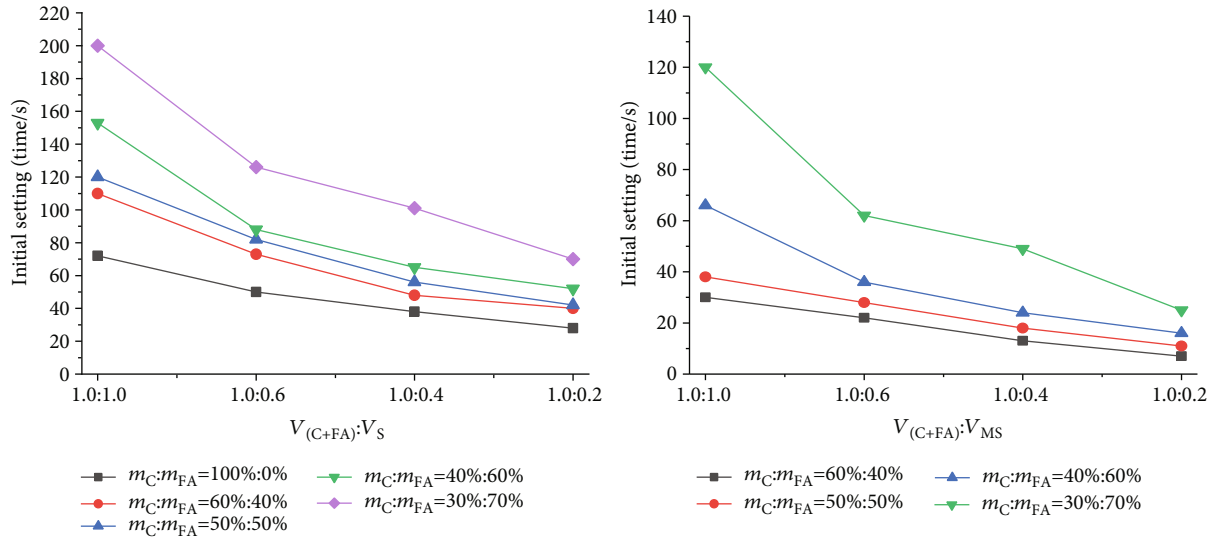

Figure 1: Curves of initial setting time. Note: $m_C : m_{FA}$ is the mass ratio of cement to fly ash in the solid powder; $V_{(C+FA)} : V_S$ is the volume ratio of the C-FA slurry to the pure S solution, and $V_{(C+FA)} : V_{MS}$ is the volume ratio of the C-FA slurry to the MS solution.

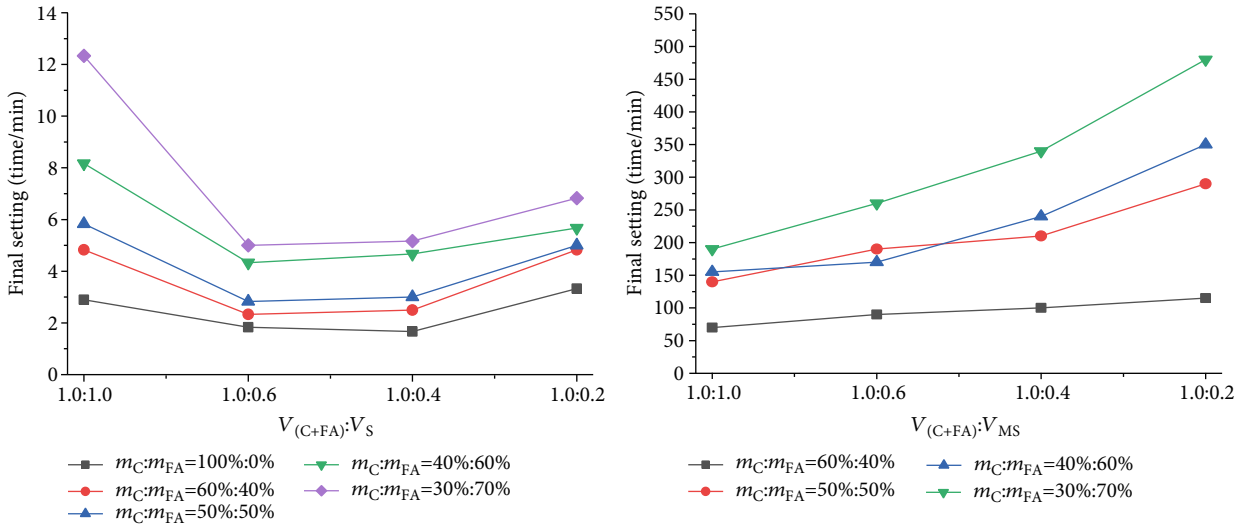

Figure 2: Curves of the final setting time. Note: $m_C : m_{FA}$ is the mass ratio of cement to fly ash in the solid powder; $V_{(C+FA)} : V_S$ is the volume ratio of the C-FA slurry to the pure S solution, and $V_{(C+FA)} : V_{MS}$ is the volume ratio of the C-FA slurry to the MS solution.

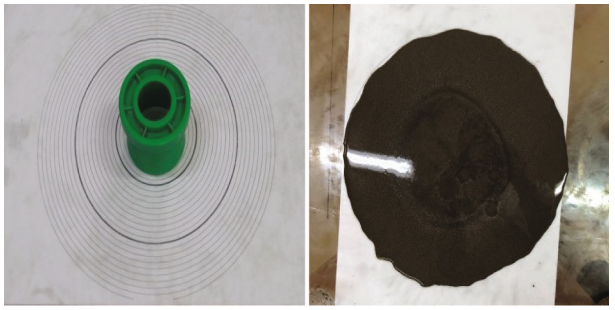

Figure 3: Determination of fluidity.

when $m_C : m_{FA} = 60\% : 40\%$, the compressive strength increased from 1.855 to 2.431 MPa and then decreased to 0.688 MPa. In addition, in the cement-fly ash-modified sodium silicate slurry system (such as $V_{(C+FA)} : V_{MS} = 1.0 : 0.6$), as the mass proportion of fly ash increased from 40 to 50, 60, and 70%, the peak compressive strength decreased from 2.431 to 1.798, 1.488, and 1.045 MPa.

Based on the above data, we conclude that when the content of sodium silicate was relatively low, $Na_2O{\cdot}nSiO_2$ quickly reacted with CaO, Al_2O_3, and other components in the powder to form $3CaO{\cdot}SiO_2$, $3CaO{\cdot}Al_2O_3$, and $4CaO{\cdot}Al_2O_3{\cdot}Fe_2O_3$, which greatly improved the early compressive strength of the solidified body. For the cement-fly ash-modified sodium silicate slurry system, when V_{MS} decreased from 1.0 to 0.6, in addition to the above, calcium oxalate

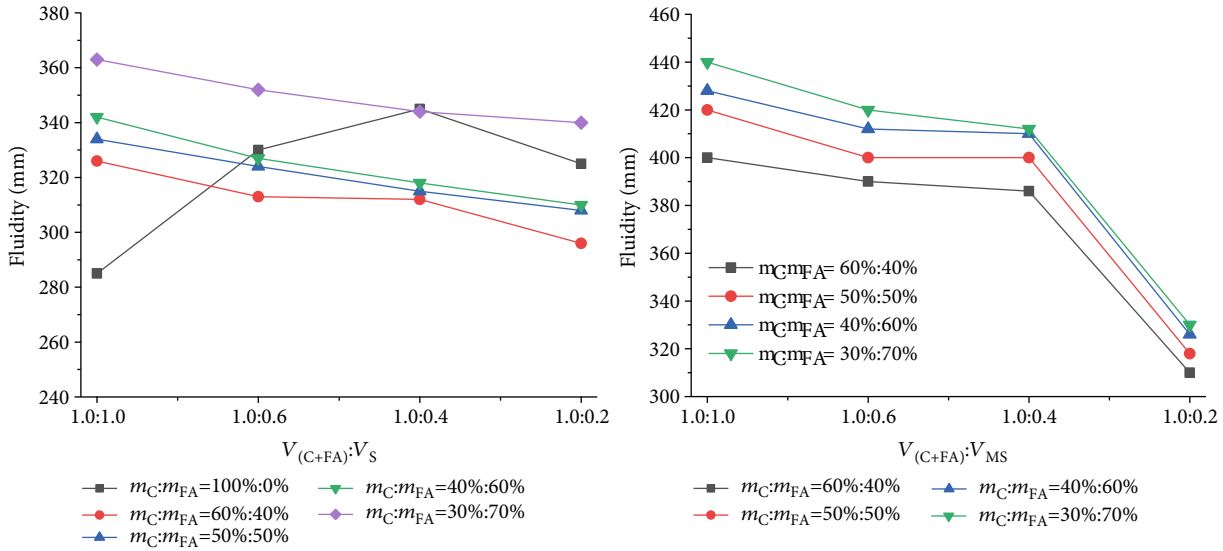

Figure 4: Curve of fluidity. Note: $m_C : m_{FA}$ is the mass ratio of cement to fly ash in the solid powder; $V_{(C+FA)} : V_S$ is the volume ratio of the C-FA slurry to the pure S solution, and $V_{(C+FA)} : V_{MS}$ is the volume ratio of the C-FA slurry to the MS solution.

Figure 5: Determination of compressive strength.

(CaC_2O_4) was also generated, which enhanced the strength of the consolidation. However, when the V_{MS} was reduced from 0.6 to 0.2, the content of $Na_2O{\cdot}nSiO_2$, $(CH_2OH)_2$, and $C_2H_2O_4$ decreased dramatically, ultimately decreasing the early compressive strength of the consolidate.

2.6. Microstructure Analysis. The cement-sodium silicate, cement-fly ash-sodium silicate, and cement-fly ash-modified sodium silicate solidified bodies cured for 7 d were dried at 20–25°C for 1 d and made into specimens with side lengths < 8 mm and thicknesses < 5 mm. The microstructures were analysed using scanning electron microscopy (SEM) with an acceleration voltage of 5 kV, as shown in Figure 7.

The microstructures of the 36 groups of samples were observed using SEM. Images at magnifications of 500, 1000, 2000, and 4000 times for No. 3 ($m_C : m_{FA} = 100\% : 0\%$ and $V_C : V_S = 1.0 : 0.4$), No. 7 ($m_C : m_{FA} = 60\% : 40\%$ and $V_{(C+FA)} : V_S = 1.0 : 0.4$), and No. 23 ($m_C : m_{FA} = 60\% : 40\%$ and $V_{(C+FA)} : V_{MS} = 1.0 : 0.4$) are shown in Figures 8(a)–8(d), respectively.

When the microstructure of the specimen surface was observed, it was found that most of the concretions in No. 3 were the products of the cement hydration reaction. The cement-sodium silicate concretions approximated a system with a dense structure but many cracks. Fly ash particles were observed on the surface of the solidified bodies in No. 7, and some fly ash particles had rough surfaces and were not completely crosslinked with the surrounding structure. The cracks on the surface of the solidified bodies were fewer than those in case of No. 3, the gel filling in the gaps was low, and the structure of the cement-fly ash-sodium silicate concretions was loose. Spherical fly ash particles with smooth and rough surfaces were uniformly dispersed in the solidified bodies in No. 23, which was closely crosslinked with the surrounding structure. In contrast with those in No. 7, most of the gaps in No. 23 were filled with a gel, and the overall structure of cement-fly ash-modified sodium silicate was relatively dense. This also explained the results of the compressive strength test from another perspective. The structure of the cement-sodium silicate solidified body was compact, and although it had several cracks, it would not be completely exposed under maintenance conditions. Hence, its compressive strength can reach 10.74 MPa. The strength of the cement-fly ash-sodium silicate solidified body decreased sharply to 0.53 MPa due to the addition of fly ash, which destroyed the dense structure of the cement-sodium silicate gel and reduced the relative content of CaO and other skeleton structures. The strength of the new cement-fly ash-modified sodium silicate solidified body increased to 1.46 MPa when pure sodium silicate was replaced with modified sodium silicate. This was because calcium oxalate (CaC_2O_4) was also generated, which enhanced the internal crosslinking and improved the compactness of the overall structure of the solidified body.

2.7. Elemental Analysis. To determine the elemental composition of the new cement-fly ash-modified sodium silicate

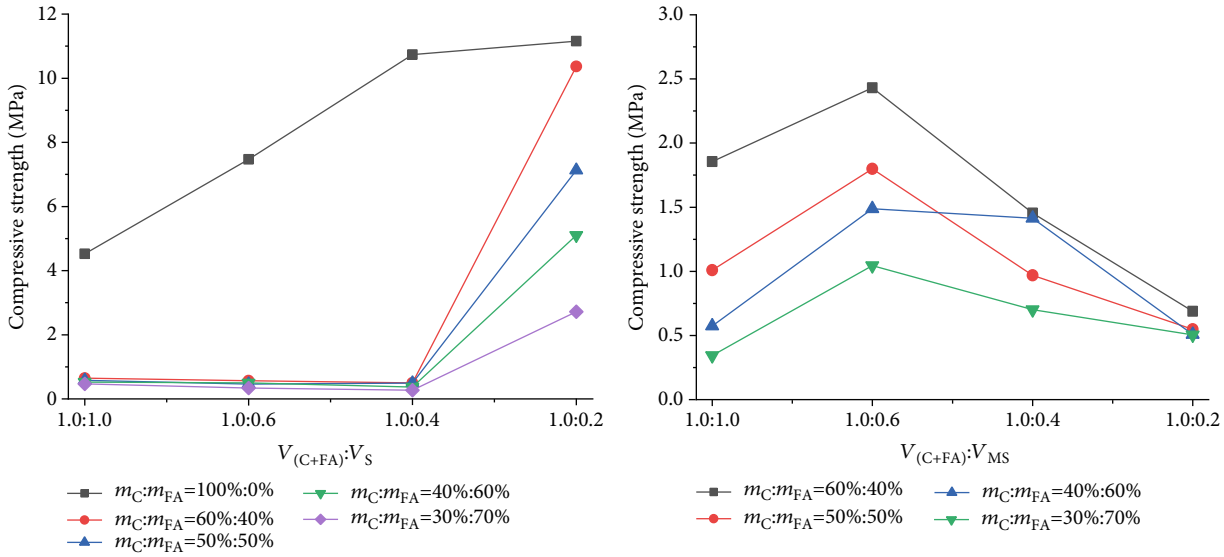

Figure 6: Compressive strength curve. Note: $m_C : m_{FA}$ is the mass ratio of cement to fly ash in solid powder; $V_{(C+FA)} : V_S$ is the volume ratio of cement-fly ash slurry to pure sodium silicate solution; $V_{(C+FA)} : V_{MS}$ is the volume ratio of cement-fly ash slurry to modified sodium silicate solution.

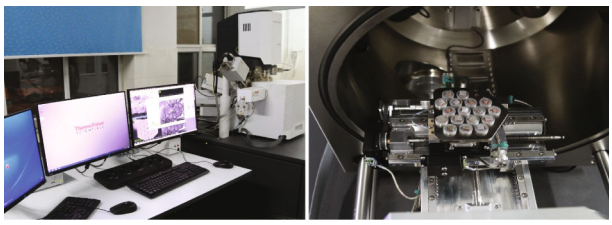

Figure 7: The picture of SEM.

material, elemental distribution characterisation and point element analysis of the C-FA-MS solidified bodies were conducted for No. 21 to No. 36. This study considers No. 34 ($m_C : m_{FA} = 30\% : 70\%$ and $V_{(C+FA)} : V_{MS} = 1.0 : 0.6$) as an example. The results are shown in Figures 9 and 10 and in Table 7.

The solidified bodies in the selected area mainly comprised O, Al, and Si along with a small amount of C, Mg, and Ca, indicating that the solidified body structure in the selected area mainly comprised aluminium acid and silicate. Carbon was mainly distributed around cracks, and the main source of carbon was modified sodium silicate, indicating that modified sodium silicate had a favourable promoting effect on repairing cracks and reducing cracks. The point element analysis showed that there was a large difference in the composition distribution of the four points, indicating that the chemical reaction processes of each section were inconsistent; moreover, the difference in the generated products was also considerable, which may also be the main reason for the decrease of 0.42 MPa in the compressive strength than that of No. 23.

2.8. Cost Analysis. Cost analysis is an important part of project cost management. In particular, the volume of various materials consumed in the goaf filling treatment was large. Therefore, greatly reducing the unit price of materials while ensuring their desirable properties has become a decisive factor in the selection of goaf treatment technologies.

Based on the grout mix ratio obtained from laboratory tests, the initial setting time of grout required for goaf engineering should be in the range of 15–80 s, final setting time should be in the range of 3–240 min, and compressive strength should not be less than 0.8 MPa after 7 days. Determining the best mix, Nos. 4 ($m_C : m_{FA} = 100\% : 0\%$ and $V_C : V_S = 1.0 : 0.2$), 20 ($m_C : m_{FA} = 30\% : 70\%$ and $V_{(C+FA)} : V_S = 1.0 : 0.2$), 31 ($m_C : m_{FA} = 40\% : 60\%$ and $V_{(C+FA)} : V_{MS} = 1.0 : 0.4$), and 34 ($m_C : m_{FA} = 30\% : 70\%$ and $V_{(C+FA)} : V_{MS} = 1.0 : 0.6$) were selected to analyse their cost based on a unit grouting volume. The results are presented in Table 8.

Table 8 shows that compared with the cement-sodium silicate slurry (No. 4), the cement-fly ash-modified sodium silicate slurry (No. 31) can provide cost savings of 44.7% ((496.40 – 274.48)/496.40). Compared to that of the cement-fly ash-sodium silicate slurry (No. 20), the cost of No. 31 can be reduced by 31.3% ((399.30 – 274.48)/399.30). The new grouting material of cement-fly ash-modified sodium silicate (C-FA-MS) can significantly reduce the engineering cost and improve the utilisation rate of solid waste, and each performance meets the needs of grouting engineering, which can be popularised in practical engineering.

For an optimal cost ratio, No. 31 was selected, wherein $m_C : m_{FA} = 40 : 60\%$ and $V_{(C+FA)} : V_{MS} = 1.0 : 0.4$. For a comparative analysis with the C-FA-S slurry, No. 37 was selected, wherein $m_C : m_{FA} = 25 : 75\%$, $m_S = 1.5\% \times (m_C + m_{FA})$, and the water – cement and fly ash ratio = 1.0 : 1.0 [23]. For the slurry, No. 38 was selected, wherein $m_C : m_{FA} = 10 : 90\%$, $m_S = 15\% \times (m_C + m_{FA})$, and the water – cement and fly ash ratio = 1.0 : 1.0 [24]. The results are presented in Table 9.

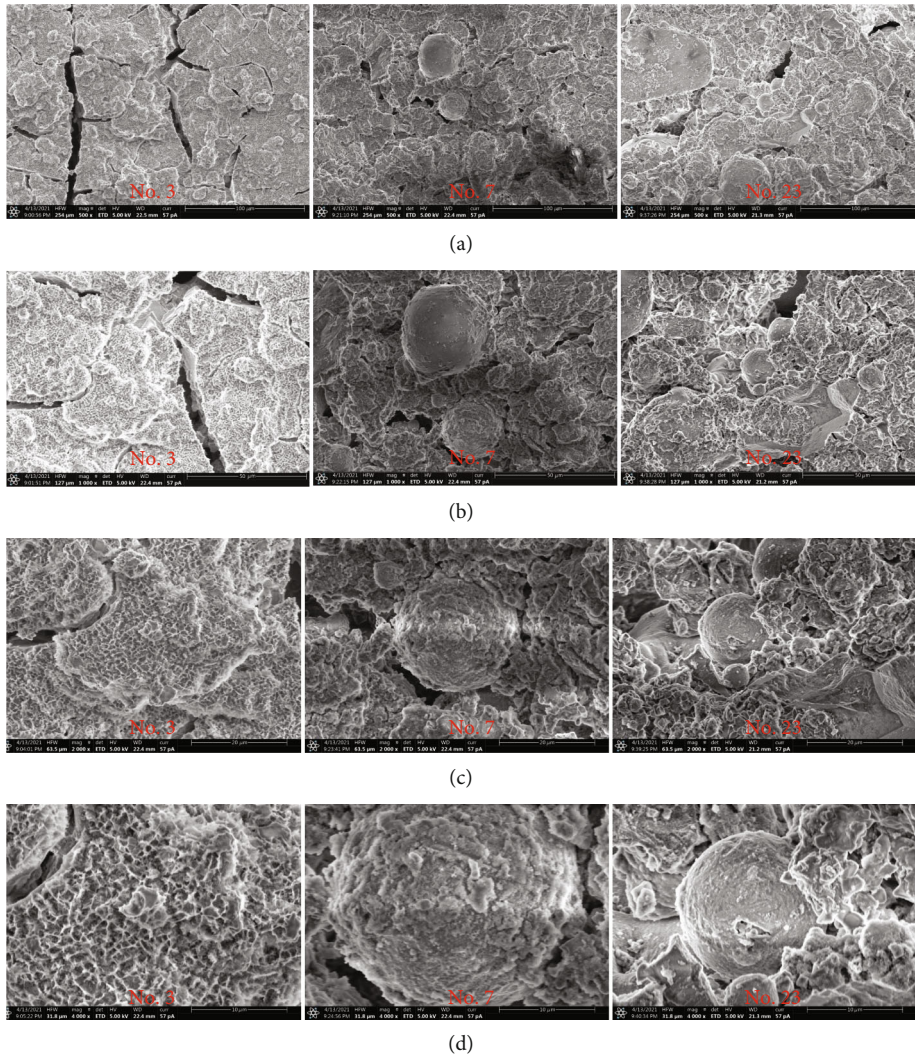

Figure 8: SEM images: (a) 500, (b) 1000, (c) 2000, and (d) 4000 times.

Table 9 shows that compared to the foreign C-FA-S slurries (Nos. 37 and 38), the C-FA-MS slurry (No. 31) is the better choice. Although the cost of this material is slightly higher, the initial setting time is lower, and it can meet the time requirements of the project.

3. Field Tests

3.1. Engineering Overview. In recent years, Shandong Province has planned to form an expressway network of "five vertical, four horizontal, one ring, and eight links." The highway from Lan Shan to He ze is an important link in the expressway network. The expressway is approximately 400 km long, passing through 21 counties and cities, such as Ri zhao and Lin yi. However, it passes the goaf left over when passing through the Wu Sizhuang coal mine in Lin yi. The exploitation depth of the Wu Sizhuang coal mine is 20–100 m. Affected by faults and geological conditions, there is an extremely uneven distribution of coal seam thickness in this area. The remaining goaf of the Wu Sizhuang coal mine was initiated in 1995 and was distributed in a north–south

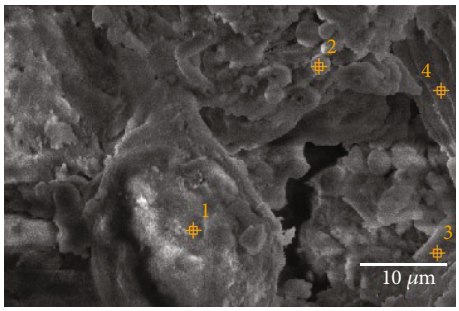

Figure 9: Element analysis point diagram.

direction. The maximum subsidence depth was 3–4 m, and it was still active, especially in the section of K92+050–K93+150. The surface deformation is evident, and large subsidence pits and cracking of houses are visible (Figure 11).

Due to the complexity of hydrogeology in this area and ambiguity of the remaining roadways in the mining area, the goaf treatment faces the following technical problems:

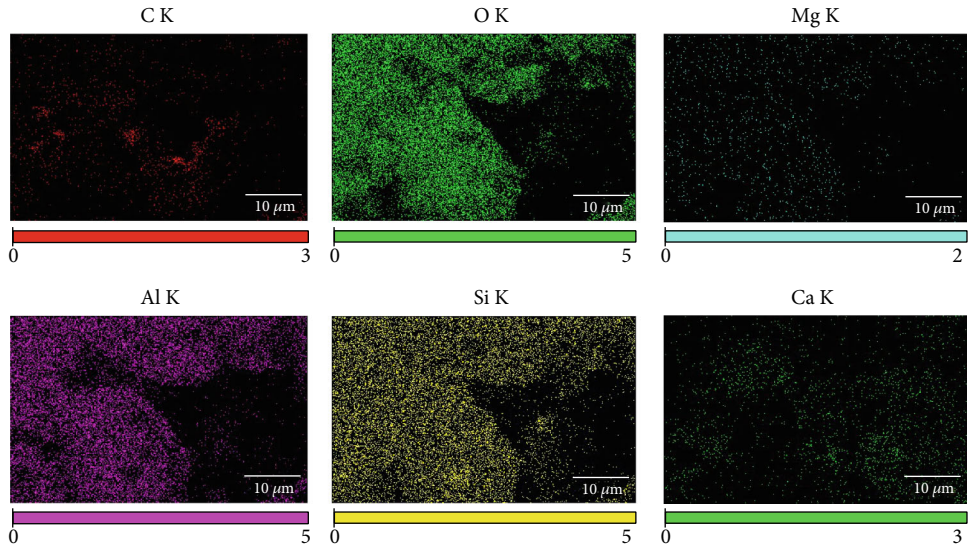

Figure 10: Distribution of element analysis.

Table 7: Analysis atomic percentage of elements at different points.

Point	C	O	Mg	Al	Si	Ca	Na	Fe
1	1.60	67.11	0.33	14.61	15.65	0.34	0.14	
2	3.21	58.33	0.52	16.43	18.04	1.27	0.53	1.26
3	2.25	31.23		5.05	7.43	54.04		
4	5.79	32.81		28.54	26.00	6.86		

(1) The amount of grouting is difficult to control. Owing to the large depth, wide range, and strong connectivity of the goaf roadway, the slurry is easily lost in large quantities, and the goaf cannot be effectively filled

(2) *High Requirements for Antidispersity of the Slurry*. The mined-out area is always waterlogged and contains impurities, which affect the gel solidification of the slurry.

(3) *Difficulty in Evaluating the Effects*. The distribution of the coal seam in the mining area is uneven; the drilling construction and coring detection are difficult.

In view of the characteristics and needs of this project, to solve the key technical problems in the treatment of the left goaf, a new cement-fly ash-modified sodium silicate (C-FA-MS) was applied for field filling grouting tests.

3.2. Grouting Reinforcement Scheme

3.2.1. Grouting Materials and Ratio. P.O.42.5-grade ordinary Portland cement produced by Linyi Zhonglian Cement Co., Ltd. (the company is located in Chewang Town, Linyi City, Shandong Province) was selected, and its performance met the requirements of General Portland Cement (GB 175-2007). The fineness of fly ash was 43 μm, and its density was approximately 2.4 g/cm^3. The modulus of sodium silicate was 2.4–3.0, Baume degree was ≥30°Bé, and purity of ethylene glycol was ≥99%.

Based on the results of laboratory tests and considering the requirements of large-volume treatment costs corresponding to the goaf, the material ratio of No. 31 (water – solid ratio = 1.0 : 1.0, $m_C : m_{FA} = 40\% : 60\%$, and $V_{(C+FA)} : V_{MS} = 1.0 : 0.4$) was selected.

3.2.2. Determination of Process Parameters

(1) *Grouting Pressure*. The grouting pressure was related to the stratigraphic configuration, buried depth of the mined-out area, and slurry fluidity [25]. Through field tests, the grouting pressure of this project was determined to be approximately 1.0–1.2 MPa. A forward grouting method was adopted under the specified grouting pressure.

(2) *The Slurry Diffusion Radius and Hole Spacing*. In the side wall of the grouting pipe, holes were made in the shape of a plum blossom, through which the grout was injected into the soil and diffused in a columnar form. The grouting hole spacing should make the grouting diffusion range of adjacent holes partially coincide to permit the reinforced rock and soil mass to form a complete stress system [26]. According to the cylindrical diffusion theory, the formula for calculating the slurry diffusion radius and hole spacing is as follows:

$$r_1 = \sqrt{\frac{2kh_1 t}{\beta n \ln\left(r_1/r_0\right)}}, \tag{1}$$

$$y = 2\sqrt{r_1^2 - \frac{b^2}{4}}, \tag{2}$$

Table 8: Cost analysis table.

No.	Grouting amount/m^3	Raw material type and component unit price					Cost
		Cement 400.0 RMB/t	Fly ash 180.0 RMB/t	Sodium silicate 1200.0 RMB/t	Ethylene glycol 4.5 RMB/kg	Adipic acid 6.0 RMB/kg	RMB
4	1	232.40		264.00			496.40
20	1	66.00	69.30	264.00			399.30
31	1	75.60	50.94	120.00	9.40	18.54	274.48
34	1	50.00	52.38	160.80	12.15	24.00	299.33

Note: Pure cement slurry density $\rho_C = 1.40$ g/cm^3; cement-fly ash slurry density $\rho_{(C+FA)} = 1.33$ g/cm^3. Pure sodium silicate density $\rho_S = 1.29$ g/cm^3; modified sodium silicate density $\rho_{MS} = 1.09$ g/cm^3.

Table 9: Cost analysis.

No.	Grouting amount/m^3	Raw material type and component unit price					Cost	Initial setting time
		Cement 400.0 RMB/t	Fly ash 180.0 RMB/t	Sodium silicate 1200.0 RMB/t	Ethylene glycol 4.5 RMB/kg	Adipic acid 6.0 RMB/kg	RMB	min
31	1	75.60	50.94	120.00	9.40	18.54	274.48	0.5
37	1	66	89.1	12	-	-	167.1	155
38	1	24.8	100.44	111.6	-	-	236.89	50

Figure 11: Ground collapse caused by goaf.

Figure 12: Field grouting.

Figure 13: H-3 core before grouting treatment.

(a) Check hole collapse (b) W1-10 core after grouting

(c) New material solidified body

Figure 14: Drilling detection of grouting effect.

Figure 15: FET audiofrequency magnetotelluric instrument and field test.

where k is the permeability coefficient ($6.2 \times 10^{-2} - 1.8 \times 10^{-1}$ cm/s), h_1 is the grouting pressure head (m), t is the grouting time (s), and β is the ratio of slurry viscosity to water viscosity (dimensionless, 0.48–0.64). Further, n is the porosity (0.4–0.5), r_1 is the slurry diffusion radius (cm), r_0 is the radius of the grouting pipe (7.5 cm), y is the hole spacing (cm), and b is the thickness of the intersecting circle of the slurry diffusion range in the adjacent holes (m) and $b = r_1$.

According to Equations (1) and (2), $k = 1.21 \times 10^{-1}$ cm/s, $h_1 = 110$ m, $t = 2$ h $= 7200$ s, $\beta = 0.56$, $n = 0.45$, and $r_0 = 7.5$ cm. The calculated slurry diffusion radius $r_1 = 3.50$ m and hole spacing $y = 6.00$ m (taking the median value of each parameter).

(3) *Grouting Volume*. The grouting volume should be calculated considering the filling volume, filling degree, and slurry loss in the mining subsidence area. The calculation formula for the single hole grouting volume is as follows:

$$Q = \pi r_1^2 L \cdot n \cdot \lambda, \tag{3}$$

where Q is the single-hole grouting volume (m^3), L is the length of the grouting section and is designed to be 6 m in this project, n is the porosity (0.4–0.5), and λ is the slurry loss coefficient (1.1–1.2) [7, 25].

According to Equation (3), the single hole grouting volume is 119.43 m^3 (taking the median value of each parameter), and it should be dynamically adjusted according to the field grouting situation.

(4) *Ending Grouting Conditions*. The end conditions of each treatment section should be comprehensively determined according to grouting volume, grouting pressure, and injection rate.

(1) Under the maximum grouting pressure, after the injection rate was <2 L/min, the grouting was screened for 20 min, and the average injection rate during the grouting period was no more than 2 L/min

(2) The unit grouting volume reaches the maximum value specified in the design

3.3. Grouting Process. In this project, first, a geological drilling machine was used to drill holes, and then, the grouting pipe was vertically imported into the borehole and sealed at the orifice. Grouting was conducted based on the order of the first edge and then the centre. When the slurry burst occurred near the grouting hole, grouting was stopped, and plugging was performed immediately. After grouting, the grouting hole was sealed with concrete mortar after slurry solidification. The grouting site is illustrated in Figure 12.

3.4. Evaluation of Grouting Effect. Before the treatment of the underlying goaf, drilling coring was conducted. The rock mass in the goaf was broken, and the distribution of hidden holes was concentrated. For example, in the H-3 hole (Figure 13), drilling to a depth of 23 m was normal. The drill dropped 40 cm at a depth of 23 m. The slurry leakage at a depth of 24–25 m indicated that the strata were broken and were determined as the roof position of the goaf. The mud wall protection method was then used to continue drilling to a depth of 27 m, and it was found that the strata gradually became complete, and the colour gradually became shallow, indicating that this location was the floor of the goaf.

Table 10: Changes in potential difference before and after goaf reinforcement.

Measuring line code	Before reinforcement			After reinforcement			Increase multiples
	Max. value	MIN value	Average value	Max. value	MIN value	Average value	
A	20.032	0.451	1.706	15.318	2.5	4.59	2.69
B	16.37	0.094	1.517	13.006	2.0	3.82	2.52
C	5.62	0.212	3.942	20.399	5.57	15.65	3.97

Note: The average value of each measuring line was calculated from 17 sets of data.

The grouting effect was detected through drilling holes 21 d after the grouting treatment. A total of 78 inspection holes (total footage 3156 m) were constructed, of which, 1 inspection hole occurred surface subsidence with an area of 2.5×2.5 m at a depth of approximately 2 m (in Figure 14(a)). The remaining 77 inspection holes passed through the collapse reinforcement area (depth = 35 – 45 m and height = 1 – 4 m), but the drill drop was significantly reduced, and the borehole wall was stable, indicating that most of the goaf collapse areas had been filled and reinforced. After grouting, drilling for cores and new material solidified bodies (i.e., drilling detection of the grouting effect) was performed, as shown in Figures 14(b) and 14(c).

Furthermore, the FET audiofrequency magnetotelluric instrument (Figure 15) was used to detect the filling degree of the target area. Three lines were arranged in the detection area. According to the principle that electromagnetic waves with different frequencies have different yield depths in a conductive medium [27], 17 groups of resistivity were recorded in each line. In the audiofrequency magnetotelluric method, the apparent resistivity can be used to infer geological conditions of the target area. It is calculated using the Cagniard formula [28] with parameters such as the emission frequency, potential difference between receiving electrodes, and horizontal magnetic field component. Therefore, the potential difference between receiving electrodes was directly used in this study to infer the regional geological conditions of the target area. The change in potential difference before and after treatment of the target area is shown in Table 10.

The electrical properties were relatively uniform when the ground layer was relatively intact, and the potential difference changed negligibly. When the mined-out area was filled with water, its potential difference was considerably lower than that of the surrounding rock. Table 10 shows that the maximum and minimum potential difference before the reinforcement was 20.023 and 0.094, respectively. After reinforcement, the maximum and minimum potential difference was 20.399 and 2.0, respectively. After goaf treatment, the potential difference of each measuring line increased by more than 2.52 times, indicating that the overall strength of the target area after reinforcement improved, and the regional integrity and uniformity significantly improved.

4. Conclusions

In this study, a new cement-fly ash-modified sodium silicate (C-FA-MS) material was studied through laboratory tests and field tests. It was concluded that the new material had evident advantages over the traditional grouting material in terms of setting time control, reinforced strength improvement, and treatment cost control. The detailed findings are as follows.

(1) The initial setting time of the slurry decreased with a decrease in the volume ratio of pure sodium silicate (V_S) or modified sodium silicate (V_{MS}). When V_S and V_{MS} were both 0.2, the initial setting time of the slurry was the shortest (cement-fly ash-modified sodium silicate slurry was 7 s). Under specific ratio conditions, the initial setting time of the cement-fly ash-modified sodium silicate slurry was shorter than that of the cement-sodium silicate and cement-fly ash-sodium silicate slurries. The final setting time of the cement-sodium silicate and cement-fly ash-sodium silicate slurries decreased first and then increased with decrease in V_S, while that of the cement-fly ash-modified sodium silicate slurry increased with decrease in V_{MS}. The mass content of fly ash in the powder was positively correlated with the initial and final setting periods of the slurry

(2) The fluidity of the cement-sodium silicate slurry first increased and then decreased with decrease in V_S. Under different fly ash content ratios, the fluidities of the cement-fly ash-sodium silicate and cement-fly ash-modified sodium silicate slurries decreased with decrease in V_S or V_{MS}. Under certain conditions, the fluidity of the cement-fly ash-modified sodium silicate slurry was greater than that of the cement-fly ash-sodium silicate and cement-sodium silicate slurries

(3) With a decrease in V_S, the overall compressive strength of the cement-sodium silicate solidified body increased up to 11.156 MPa. When V_S decreased from 0.4 to 0.2, the compressive strength of the cement-fly ash-sodium silicate slurry increased significantly, up to 10.369 MPa. With the decrease in V_{MS}, the compressive strength of the cement-fly ash-modified sodium silicate solidified body first increased and then decreased (when $m_C : m_{FA} = 60\% : 40\%$, the compressive strength increased from 1.855 to 2.431 MPa and then decreased to 0.688 MPa). There was a negative correlation between the fly ash weight and solidified body strength

(4) The microstructure of the cement-sodium silicate concretions was compact but had several cracks. The fly ash in the cement-fly ash-sodium silicate

solidified body destroyed the compact structure of the cement-sodium silicate concretions and reduced the relative contents of CaO and other skeletal structures. Calcium oxalate CaC_2O_4 was generated in the cement-fly ash-modified sodium silicate solidified body, which enhanced the internal crosslinking of the gel and improved the strength of the solidified body

(5) Under the condition of unit grouting amount, the cost of the cement-fly ash-modified sodium silicate slurry was approximately 44.7% lower than that of the cement-sodium silicate slurry and approximately 31.3% lower than that of the cement-fly ash-sodium silicate slurry. After the treatment of the underlying mined-out area, the borehole coring test showed that most of the mined-out subsidence areas had been filled and strengthened. The FET magnetotelluric exploration showed that the increase in the potential difference of each line was more than 2.52 times, indicating that the regional integrity and uniformity had been significantly improved

Data Availability

The data used to support the findings of this study are available from the corresponding author upon request.

Conflicts of Interest

The authors declare that there are no conflicts of interest regarding the publication of this paper.

Acknowledgments

This study was financially supported by the National Natural Science Foundation of China (Grant No. 52009075), the Natural Science Foundation of Shandong Province of China (Grant Nos. ZR2020QE262 and ZR2020QE291), and the Doctoral Research Fund of Shandong Jianzhu University (Grant Number X19018Z).

References

[1] S. Xugen, L. Xiumin, C. Congxin et al., "Study on the mechanism of surface collapse and ground deformation in western mined area of of Chengchao iron mine," *Chinese Journal of Rock Mechanics and Engineering*, vol. 37, no. S2, pp. 4262–4273, 2018, (in Chinese).

[2] Z. F. Zhou, H. D. Cao, and M. C. Zhu, "Application of cement-sodium silicate mixed grout in control of water and sand bursting from roof of the working face," *Coal Geology & Exploration*, vol. 46, no. 6, pp. 121–127, 2018, (in Chinese).

[3] A. Estokova, M. Kovalcikova, A. Luptakova, and M. Prascakova, "Testing silica fume-based concrete composites under chemical and microbiological sulfate attacks," *Materials*, vol. 9, no. 5, pp. 324–334, 2016.

[4] D. Ma, J. Zhang, H. Duan et al., "Reutilization of gangue wastes in underground backfilling mining: overburden aquifer protection," *Chemosphere*, vol. 264, Part 1, pp. 128400–128413, 2021.

[5] D. Ma, J. Wang, X. Cai et al., "Effects of height/diameter ratio on failure and damage properties of granite under coupled bending and splitting deformation," *Engineering Fracture Mechanics*, vol. 220, pp. 106640–106654, 2019.

[6] R. T. Liu, Z. Zheng, S. C. Li, and H. L. Yang, "Mechanical properties of fractured rock mass with consideration of grouting reinforcement," *China Journal of Highway and Transport*, vol. 31, no. 10, pp. 284–291, 2018, (in Chinese).

[7] Z. Qing-song, Z. Lian-zhen, L. Ren-tail et al., "Laboratory experimental study of cement-silicate slurry diffusion law of crack grouting with dynamic water," *Rock and Soil Mechanics*, vol. 36, no. 8, pp. 2159–2168, 2015, (in Chinese).

[8] D. Y. Xuan, J. Li, K. D. Zheng, and J. Xu, "Experimental study of slurry flow in mining-induced fractures during longwall overburden grout injection," *Geofluids*, vol. 2020, Article ID 8877616, 10 pages, 2020.

[9] G. Girskas, O. Kizinievič, and V. Kizinievič, "Analysis of durability (frost resistance) of MSWI fly ash modified cement composites," *Archives of Civil and Mechanical Engineering*, vol. 21, no. 2, pp. 34–52, 2021.

[10] P. Górak, P. Postawa, L. N. Trusilewicz, and A. Kalwik, "Cementitious eco-composites and their physicochemical/mechanical properties in Portland cement-based mortars with a lightweight aggregate manufactured by upcycling waste by-products," *Journal of Cleaner Production*, vol. 289, pp. 125–136, 2020.

[11] G. Hu, W. He, and C. Lan, "Sealing behavior and flow mechanism of expandable material slurry with high water content for sealing gas drainage boreholes," *Geofluids*, vol. 2018, Article ID 2954306, 15 pages, 2018.

[12] G. Sukmak, P. Sukmak, S. Horpibulsuk et al., "Physical and mechanical properties of natural rubber modified cement paste," *Construction and Building Materials*, vol. 244, pp. 118319–119129, 2020.

[13] S. J. Ma and D. P. Ma, "Grouting material for broken surrounding rock and its mechanical properties of grouting reinforcement," *Geotechnical and Geological Engineering*, vol. 39, pp. 17–25, 2021.

[14] M. Kumar, N. P. Singh, and S. K. Singh, "Effect of polycarboxylate type of super plasticizer on the hydration properties of composite cements," *Frontiers of Chemistry in China*, vol. 6, no. 1, pp. 201–210, 2011.

[15] C. Wang, Z. Q. Xiong, C. Wang, Y. Wang, and Y. Zhang, "Study on rib sloughage prevention based on geological structure exploration and deep borehole grouting in front abutment zones," *Geofluids*, vol. 2020, Article ID 7961032, 12 pages, 2020.

[16] F. Celik and O. Akcuru, "Rheological and workability effects of bottom ash usage as a mineral additive on the cement based permeation grouting method," *Construction and Building Materials*, vol. 263, pp. 120186–120218, 2020.

[17] X. Guan, H. B. Zhang, Z. P. Yang et al., "Research of high performance inorganic-organic composite grouting materials," *Journal of China Coal Society*, vol. 45, no. 3, pp. 902–910, 2020, (in Chinese).

[18] B. Y. Liu, "Test and applied research on sodium silicate grouting materials of polyester fiber modified composite cement-base," *Municipal Engineering Technology*, vol. 37, no. 5, pp. 252–255, 2019, (in Chinese).

[19] A. Bodocsi and M. T. Bowers, "Permeability of acrylate, urethane, and silicate grouted sands with chemicals," *Journal of*

Geotechnical and Geoenvironmental Engineering, vol. 117, no. 8, pp. 1227–1244, 1991.

[20] S. M, J. R, and R. N. P, "Effect of change in the silica modulus of sodium silicate solution on the microstructure of fly ash geopolymers," *Journal of Building Engineering*, vol. 44, article 102939, 12 pages, 2021.

[21] T. Mitsumata, H. Kawada, and J. Takimoto, "Thermosensitive solutions and gels consisting of poly(vinyl alcohol) and sodium silicate," *Materials Letters*, vol. 61, no. 18, pp. 3878–3881, 2007.

[22] Y. X. Li and X. J. Qin, "Application of filling grouting method in goaf control," *Coal and Chemical Industry*, vol. 39, no. 4, pp. 129–132, 2016, (in Chinese).

[23] I. Cavusoglu, E. Yilmaz, and A. O. Yilmaz, "Sodium silicate effect on setting properties, strength behavior and microstructure of cemented coal fly ash backfill," *Powder Technology*, vol. 384, pp. 17–28, 2021.

[24] M. Kermani, F. P. Hassani, E. Aflaki, M. Benzaazoua, and M. Nokken, "Evaluation of the effect of sodium silicate addition to mine backfill, Gelfill - part 2: effects of mixing time and curing temperature," *Journal of Rock Mechanics and Geotechnical Engineering*, vol. 7, no. 6, pp. 668–673, 2015.

[25] X. Feng, L. I. Shucai, R. Liu, W. HAN, and S. Zhang, "Theoretical and experimental research on the grout fronts diffusion considering filtration effect," *Scientia Sinica Technologica*, vol. 47, no. 11, pp. 1198–1206, 2017, (in Chinese).

[26] X. Feng, Q. S. Zhang, Q. C. Jiang et al., "Study on variation law of cement slurry density in porous media considering convection–diffusion–infiltration," *Arabian Journal of Geosciences*, vol. 12, no. 23, pp. 742–753, 2019.

[27] K. Li, Y. Pan, J. Xie, and H. Zhang, "Performance research and engineering application of FA-based geopolymer grouting materials," *New Building Materials*, vol. 48, no. 1, pp. 57–63, 2021, (in Chinese).

[28] L. Cagniard, "Électricité tellurique," *Geophysik I / Geophysics I*, vol. 10 / 47, no. 47, pp. 407–469, 1956.